ACS APPLIED MATERIALS & INTERFACES

RESEARCH ARTICLE

www.acsami.org

Hydrothermal Synthesis and Electrochemical Properties of $Li_3V_2(PO_4)_3$/C-Based Composites for Lithium-Ion Batteries

Chunwen Sun,[†,‡] Shreyas Rajasekhara,[†] Youzhong Dong,[†] and John B. Goodenough*[,†]

[†]Texas Materials Institute, ETC 9.184, The University of Texas at Austin, Austin, Texas 78712, United States

[‡]Beijing National Laboratory for Condensed Matter Physics, Institute of Physics, Chinese Academy of Sciences, Beijing, 100190, China

Supporting Information

ABSTRACT: To improve performance at higher rates, we developed a hydrothermal method to prepare carbon-coated monoclinic lithium vanadium phosphate ($Li_3V_2(PO_4)_3$) powder to be used as a cathode material for Li-ion batteries. The structural, morphological and electrochemical properties were characterized by X-ray diffraction (XRD), scanning and transmission electron microscopy (SEM and TEM), and galvanostatic charge−discharge cycling. A superior cycle and rate behavior are demonstrated for $Li_3V_{1.85}Sc_{0.15}(PO_4)_3$/C and $Li_{2.96}Ca_{0.02}V_2(PO_4)_3$/C electrodes at charge−discharge current rates above 5*C*.

KEYWORDS: hydrothermal synthesis, lithium vanadium phosphate, doped, lithium-ion batteries

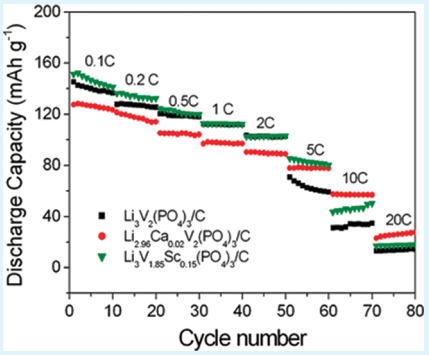

1. INTRODUCTION

Transition-metal phosphates have attracted considerable interest as the cathode material for rechargeable lithium-ion batteries. Among these phosphates, $LiFePO_4$ is considered to be an excellent candidate cathode for power batteries in electric vehicles (EVs). Its advantages include a high theoretical specific capacity (170 mA h g^{-1}), low cost, environmental compatibility, and intrinsic thermal safety.[1−7] However, it has a relatively low operation voltage of around 3.45 V versus lithium. Lithium vanadium phosphate $Li_3V_2(PO_4)_3$ (abbreviated as LVP hereafter) crystallizes in two different forms: the rhombohedral (NASICON) structure[8] and the thermodynamically more stable monoclinic phase.[9] The host framework $V_2(PO_4)_3$ forms a three-dimensional network of metal octahedra and phosphate tetrahedra sharing oxygen vertices; the guest Li^+ ions are mobile in the interstitial space. Two lithium ions can be extracted from monoclinic LVP between 3.0 and 4.3 V based on the V^{3+}/V^{4+} redox couple. When charged to 4.8 V, all three lithium ions can be completely extracted, corresponding to a theoretical capacity of 197 mA h g^{-1}. It is believed that monoclinic $Li_3V_2(PO_4)_3$ undergoes a complex series of two-phase transitions during lithium extraction and a solid solution regime on lithium reinsertion.[9] However, $Li_3V_2(PO_4)_3$ has poor electronic conductivity, which restricts its practical application for lithium-ion batteries. It is generally believed that small particle size, carbon coating, and doping of other metal ions are beneficial for improving the electrochemical properties of $Li_3V_2(PO_4)_3$.

The effects of several dopant elements on the electrochemical properties of $Li_3V_2(PO_4)_3$/C have been reported, including divalent Co[10] and Mg;[11−14] trivalent Fe,[15] Al,[16,17] Sc,[14] and Cr;[18] tetravalent Ti[13,14,19] and Zr;[20] pentavalent Nb[21,22] ions in vanadium sites; and monovalent K[14] in lithium sites in $Li_3V_2(PO_4)_3$. The monoclinic phase of $Li_3V_2(PO_4)_3$ is iso-typic with those of its scandium, iron, and chromium analogues.[23,24] However, no research on Ca doping in lithium sites in $Li_3V_2(PO_4)_3$ has been reported. Although Mateyshina et al.[14] reported recently the $Li_3V_2(PO_4)_3$ sample doped with Sc has good cycleability at a 0.1*C* rate, they did not show the high-rate performance. In this work, we investigated hydrothermal synthesis of doped $Li_3V_2(PO_4)_3$ samples in order to simplify the two-step calcinations of solid-state synthesis performed at 850 or 900 °C for a long time[9,10,16,25] and to obtain smaller particles for better high-rate performance. Dopants are thought to stabilize the monoclinic structure; both Sc and Ca dopants should increase the volume of the interstitial space, but the larger Ca^{2+} ion is substituted for Li^+ ions rather than for V^{3+} ions; a larger interstitial volume may also enhance the Li^+-ion mobility. We show that this approach increases the performance above the 5*C* rate.

2. EXPERIMENTAL SECTION

2.1. Preparation of Materials. In a typical synthesis, stoichiometric amounts of 0.01 mol of lithium acetate hydrate ($CH_3COOLi.2H_2O$), ammonium metavanadate (NH_4VO_3), and ammonium dihydrogen phosphate ($NH_4H_2PO_4$) were dissolved in 35 mL of distilled water; 2.5 mL of ethylene glycol (EG) was then added to the solution. A yellow suspension was obtained. The pH value of the yellow suspension was about 1. This solution mixture was stirred for 30 min before being transferred into a 50 mL

Received: July 27, 2011
Accepted: August 30, 2011
Published: August 30, 2011

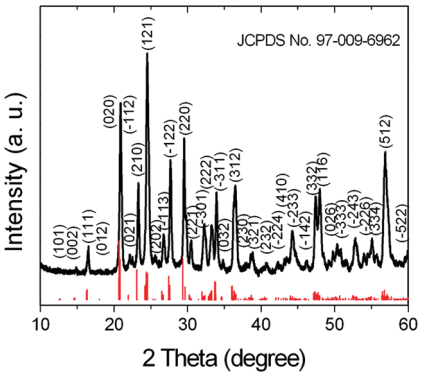

Figure 1. XRD patterns of the $Li_3V_2(PO_4)_3$/carbon prepared hydrothermally and calcined at 700 °C for 10 h.

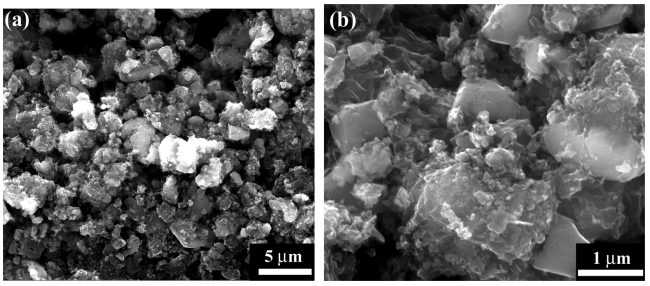

Figure 2. SEM images of the $Li_3V_2(PO_4)_3$/carbon prepared hydrothermally and calcined at 700 °C for 10 h.

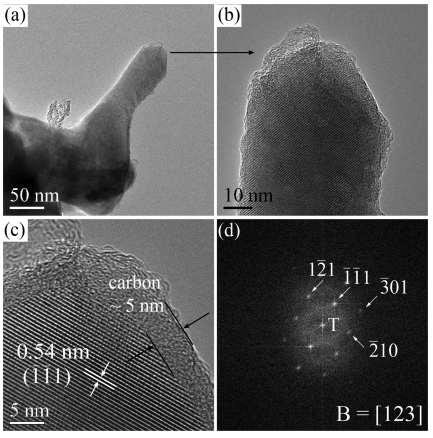

Figure 3. TEM images of $Li_3V_2(PO_4)_3$/carbon composite: (a, b) overview of $Li_3V_2(PO_4)_3$/C particle obtained at an accelerating voltage of 120 kV, (c) HRTEM image of the $Li_3V_2(PO_4)_3$/C particle that shows a continuous carbon layer, (d) analysis of the FFT pattern obtained from c; B denotes the electron-beam direction.

Teflon-lined autoclave. The autoclave was sealed, kept at 180 °C for 24 h in an electric oven, and then cooled to room temperature naturally. The blue gel suspension and black precipitate were mixed and heated on a hot plate at 80 °C under stirring to get a product. The product was coated with carbon by dispersing the powder into a sucrose solution; the amount of carbon was about 5 wt.% of the product. The powder was calcined at 700 °C for 10 h under hydrogen (5% volume)-argon. The heating rate was 3 °C min^{-1}. Before increasing the temperature, the tube furnace was evacuated for 30 min.

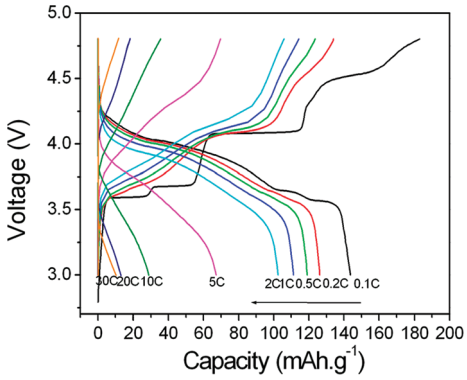

Figure 4. Typical half-cell charge/discharge curves of a $Li_3V_2(PO_4)_3$/C cathode in the potential region from 3.0 to 4.8 V at various charge and discharge current rates.

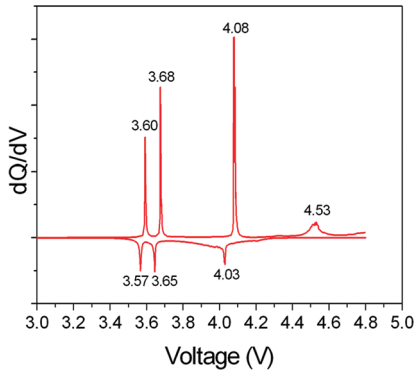

Figure 5. Differential capacity plot of a Li/$Li_3V_2(PO_4)_3$/C cell (derived from data in the first cycle).

For the Ca- and Sc-doped $Li_3V_2(PO_4)_3$, the procedures were the same as those for $Li_3V_2(PO_4)_3$ except a stoichiometric amount of calcium acetate ($Ca(C_2H_3O_2)_2$) or scandium nitrate ($Sc(NO_3)_3.xH_2O$) was added.

2.2. Characterization of Materials. X-ray powder diffraction (XRD) patterns of the calcined product were step-scan recorded on a Philips X-ray diffractometer equipped with Cu K_α radiation in steps of 0.02° with a step time of 2 s over the 2θ range of 10−70° for each sample. Scanning electron microscopy (SEM) was performed on a Quanta 650 scanning electron microscope. Transmission electron microscopy (TEM) and high resolution transmission electron microscopy (HRTEM) were carried out on a JEOL 2010F transmission electron microscope.

2.3. Electrode Fabrication and Electrochemical Tests. Electrochemical performances of each carbon-coated sample were evaluated with a standard CR2032 coin cell composed of the cathode, lithium anode, a Celgrade polypropylene separator, and $LiPF_6$ in 1:1 ethylene carbonate (EC) and diethyl carbonate (DEC) as the electrolyte. The cathode was prepared by mixing 75 wt % C−$Li_3V_2(PO_4)_3$ with 20 wt % acetylene black (Alfa Aesar) and 5 wt % polytetrafluoroethylene (PTFE) binder (G163, AGC company); the mixture was rolled into thin sheets that were punched into circular discs 0.78 cm in diameter. The loading of the active material is about 5−6 mg cm^{-2}. All cells were fabricated in an argon-filled glovebox. The cells were aged for 12 h before charge/discharge to ensure full absorption of the electrolyte into the electrode. Initially, cells were galvanostatically cycled at a low current density of 15 mA g^{-1} (about 0.1*C* rate) in an Arbin Instruments testing system

Table 1. Refined Lattice Parameters for Pure and Doped $Li_3V_2(PO_4)_3/C$

samples	a (Å)	b (Å)	c (Å)	β (deg)	V (Å^3)
$Li_3V_2(PO_4)_3/C$	8.6091(4)	8.6011(2)	12.0452(5)	90.5630(2)	891.884(8)
$Li_{2.96}Ca_{0.02}V_2(PO_4)_3/C$	8.6121(5)	8.6060(3)	12.0468(7)	90.5630(9)	892.813(8)
$Li_3V_{1.85}Sc_{0.15}(PO_4)_3/C$	8.6153(3)	8.6086(2)	12.0548(6)	90.5455(6)	894.003(7)

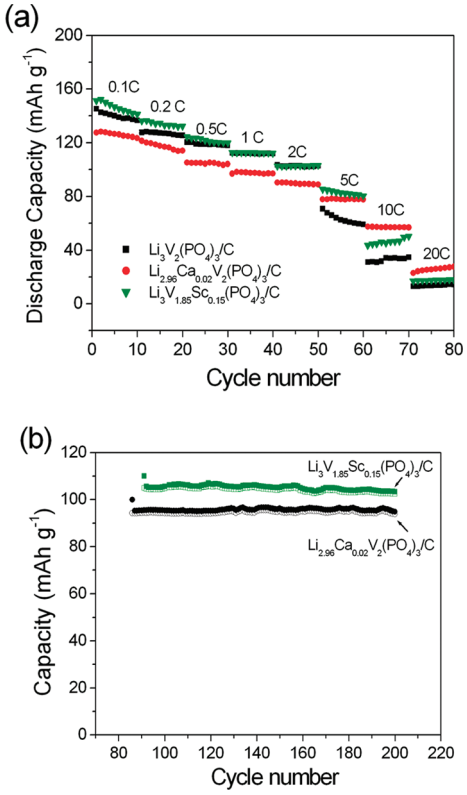

Figure 6. (a) Comparison of the rate performance of $Li_3V_{1.85}Sc_{0.15}(PO_4)_3/C$ and $Li_{2.96}Ca_{0.02}V_2(PO_4)_3/C$ with that of LVP/C at various charge and discharge current rates; (b) the cycle performance of $Li_3V_{1.85}Sc_{0.15}(PO_4)_3/C$ and $Li_{2.96}Ca_{0.02}V_2(PO_4)_3/C$ at 1*C* charge–discharge current.

(Arbin BT-2000); the current density was subsequently increased to 20 C before returning to 0.1 C. On an area specific basis, 1 C charge/discharge current is equivalent to 0.75–0.9 mA/cm^2.

3. RESULTS AND DISCUSSION

The phase purity and crystal structure of the carbon-coated product were examined by XRD. Figure 1 shows that the pattern can be indexed in the monoclinic space group $P2_1/n$. The SEM images in Figure 2 show that the particle size ranges from several hundred nanometers to several micrometers and that most of the particles are aggregated.

To clarify the microstructure of the $Li_3V_2(PO_4)_3/C$ composite, we show typical TEM and HRTEM images taken from the $Li_3V_2(PO_4)_3/C$ particles in Figure 3. For mitigating the beam damage on the sample, a low accelerating voltage of 120 kV was applied in this study instead of a typical voltage of 200 kV. The HRTEM image in Figure 3c displays clear crystal planes with a *d*-spacing of 0.54 nm, corresponding to the $(\bar{1}\,\bar{1}\,1)$ planes of monoclinic $Li_3V_2(PO_4)_3$. In addition, it is clearly seen from the HRTEM image that an amorphous carbon layer with a thickness of approximately 5 nm covered the surface of the $Li_3V_2(PO_4)_3$ particles. Figure 3d is the indexed fast Fourier transform (FFT) pattern of Figure 3c, which further confirms that the obtained $Li_3V_2(PO_4)_3$ has a monoclinic crystal structure and indicates the single-crystal character of the particle.

Figure 4 shows a typical charge/discharge profile of $Li_3V_2(PO_4)_3/C$ in the potential region from 3.0 to 4.8 V at various current rates; the initial charge/discharge data give a discharge capacity of 145 mA h g^{-1} at 0.1*C* rates, which is similar to the result at low rate of the LVP/C obtained with solid-state synthesis.[26] No data at higher rates are reported in that literature. The reversible specific capacity remains more than 60 mA h g^{-1} at 5C charge and discharge rates. If the cell is charged to 4.8 V, all three Li^+ ions are extracted from monoclinic LVP over four two-phase electrochemical plateaus at 3.60, 3.68, 4.08, and 4.53 V, which correspond to different phases of $Li_xV_2(PO_4)_3$ at x = 3.0, 2.5, 2.0, 1.0, and 0.5, respectively.[27] The first lithium ion was extracted in two steps (3.60 and 3.68 V) for the mixed V^{3+}/V^{4+} couple because of the existence of ordered phases at $Li_{2.5}V_2(PO_4)_3$ and $Li_2V_2(PO_4)_3$. Then, a single-step removal of the second lithium ion at 4.08 V can be observed, which corresponds to a 0.4 V step from the V^{3+}/V^{4+} couple to the V^{5+}/V^{4+} couple. Three plateaus at 4.03, 3.65, and 3.57 are observed during the discharge process. These plateaus correspond to the peaks in the dQ/dV plots shown in Figure 5.

We examine the effects of various contents of Sc for V and Ca for Li on the electrochemical properties of $Li_3V_{2-x}Sc_x(PO_4)_3$ with x = 0.02, 0.05, 0.1, and 0.15 as well as $Li_{3-2x}Ca_xV_2(PO_4)_3$ with x = 0.01, 0.02, and 0.03, respectively. Because the ionic radius of Sc^{3+} (0.73 Å) is larger than that of V^{3+} (0.64 Å) and the ionic radius of Ca^{2+} (1.00 Å) is larger than that of Li^+ (0.74 Å),[28] the lattice parameters of $Li_3V_2(PO_4)_3$ are expected to be increased by doping of Sc^{3+} or Ca^{2+} so as to increase the Li^+-ion mobility. From the XRD patterns, it was found that the location of the (020) diffraction peaks in the 2θ ranges of 19.5–22° shifts to lower 2θ with increasing Sc or Ca content (see Figure S1B and S4B in Supporting Information). In addition, it is noted that a little amount of $LiV(P_2O_7)$ impurity phases is segregated from the doped LVP samples (see Figure S1A and S4A in the Supporting Information). In this study, the best performance was found in the sample with x = 0.15 Sc in $Li_3V_{2-x}Sc_x(PO_4)_3/C$ and x = 0.02 Ca in $Li_{3-2x}Ca_xV_2(PO_4)_3/C$ (see Figures S3 and S6 in the Supporting Information). Table 1 summarizes the lattice parameters obtained by the Rietveld refinement of the powder X-ray diffraction data for the pure and doped $Li_3V_2(PO_4)_3/C$. It can be seen that the unit-cell volumes of $Li_{2.96}Ca_{0.02}V_2(PO_4)_3/C$ and $Li_3V_{1.85}Sc_{0.15}(PO_4)_3/C$ samples increase compared to that of pure LVP/C, indicating that Ca or Sc doping indeed cause the lattice expansion as expected.

Comparison of the rate performance of $Li_{2.96}Ca_{0.02}V_2(PO_4)_3/$carbon and $Li_3V_{1.85}Sc_{0.15}(PO_4)_3/$carbon with those of LVP/C at various current rates are shown in Figure 6a. For Sc substitution,

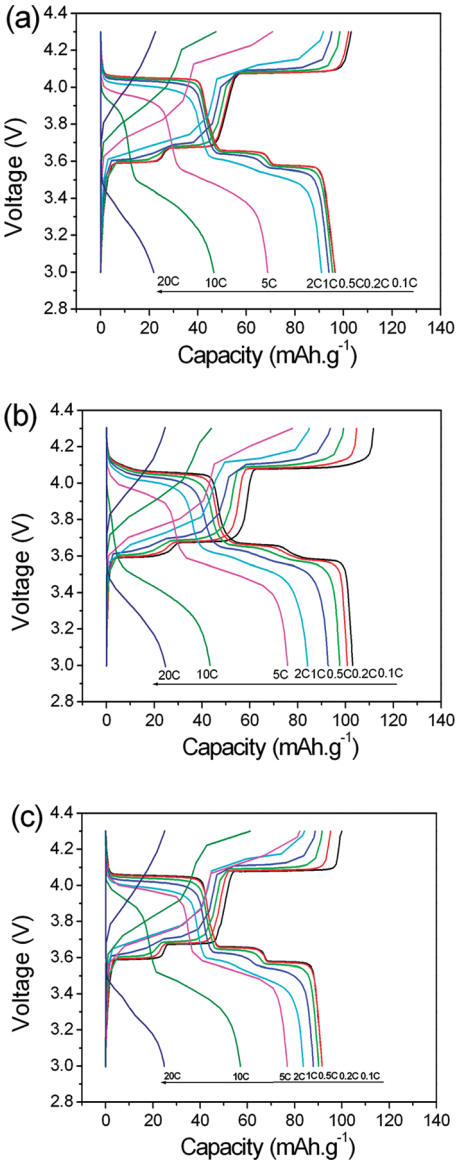

Figure 7. Typical charge/discharge curves of LVP-based electrodes in the potential region from 3.0 to 4.3 V at various charge and discharge current rates: (a) $Li_3V_2(PO_4)_3$/C; (b) $Li_3V_{1.85}Sc_{0.15}(PO_4)_3$/C; and (c) $Li_{2.96}Ca_{0.02}V_2(PO_4)_3$/C.

$Li_3V_{1.85}Sc_{0.15}(PO_4)_3$/carbon shows comparable performance to that of LVP/C sample at low rates ($\leq$2C); however, at 5C and 10C charge−discharge rate, the $Li_3V_{1.85}Sc_{0.15}(PO_4)_3$/carbon demonstrates superior behavior. For Ca substitution, the $Li_{2.96}Ca_{0.02}V_2(PO_4)_3$/C exhibits lower capacities at low rates compared with those of LVP/C; however, the $Li_{2.96}Ca_{0.02}V_2(PO_4)_3$/C shows good capacity retention capability and higher capacities at higher rates ($\geq$5C). After testing rate performance, the cells were subsequently charged and discharged at 1C rate up to 200 cycles. As shown in Figure 6b, both $Li_3V_{1.85}Sc_{0.15}(PO_4)_3$/carbon and $Li_{2.96}Ca_{0.02}V_2(PO_4)_3$/carbon display good cycle performance compared with that of Co-doped LVP reported in the literature.[10] The positive effect of Ca^{2+} and Sc^{3+} doping can be attributed to stabilization of a monoclinic structure of LVP by doping and more uniform particle morphologies (see Figures S2 and S5 in the Supporting Information), which is similar to the cases of enhanced phase stability of LVP by doping of Mg^{2+},[12] Zr^{4+},[20] or Fe^{3+}.[15]

Smaller particles obtained by hydrothermal synthesis enhance Li-ion insertion rates as well as capacity retention; however, the Coulombic efficiency is decreased in the first charge−discharge because of side reactions involving electrolyte oxidation and solid electrolyte interphase (SEI) formation at higher voltages on both amorphous carbon and acetylene black.[29−31] Measurement of the onset of the oxidation reaction of the oxide cathode with the carbonate electrolyte has given a reported HOMO of the electrolyte $LiPF_6$ in EC/DEC located at about 4.3 eV versus Li^+/Li.[32−34] For mitigating the side reactions during cycling, we also tested the charge−discharge curves in the potential region from 3.0 to 4.3 V at various charge and discharge current rates for $Li_3V_2(PO_4)_3$/C, $Li_{2.96}Ca_{0.02}V_2(PO_4)_3$/C and $Li_3V_{1.85}Sc_{0.15}(PO_4)_3$/C electrodes. As shown in Figure 7, the tests show that the lithium extraction-insertion processes are reversible and the two-phase electrochemical plateaus are obvious in the charge−discharge curves especially at low charge−discharge rates. The initial Coulombic efficiencies of all the three electrodes are improved compared to those charged−discharged in the potential region from 3.0 to 4.8 V. In addition, it was found that the high-rate performance of cells is improved by decreasing the cutoff voltage of charge to 4.3 V; but the capacities are slightly lower at low charge−discharge rates (Figure 7). The tests also indicate that the rate capability of Ca- or Sc-doped LVP/C is better than that of the original LVP/C electrode. There is an enhancement for both dopants at the 5C rate. A step change of the capacities is observed in the capacity between 2 and 5C for the original LVP/C and that moves to the higher rates for the doped samples, which may be related to the enhanced Li^+-ion mobility after doping.

4. CONCLUSIONS

A hydrothermal method has been developed to synthesize LVP/C composites with smaller particle size. The thermal treatment following the hydrothermal process was performed at a lower temperature than that of the conventional two-step solid-state reaction. By doping Sc into V sites and Ca into Li sites, superior cycle and rate behaviors are demonstrated for $Li_{2.96}Ca_{0.02}V_2(PO_4)_3$/C and $Li_3V_{1.85}Sc_{0.15}(PO_4)_3$/C electrodes at charge and discharge current rates above 5C.

■ ASSOCIATED CONTENT

Supporting Information. SEM image, XRD patterns, and the first five charge−discharge curves of $Li_3V_{2-x}Sc_x(PO_4)_3$/C and $Li_{3-2x}Ca_xV_2(PO_4)_3$/C electrodes at 0.1 C rate. This material is available free of charge via the Internet at http://pubs.acs.org.

■ AUTHOR INFORMATION

Corresponding Author

*Tel: +1-512-471-1646. Fax: +1-512-471-7681. E-mail: jgoodenough@mail.utexas.edu.

■ ACKNOWLEDGMENT

Financial support from the Energy Frontier Research Center (EFRC) of DOE, USA is acknowledged (Grant DE-SC0001091).

C. Sun is also supported by the Institute of Physics (IOP) start-up funding.

REFERENCES

(1) Padhi, A.; Nanjundaswamy, K.; Goodenough, J. B. *J. Electrochem. Soc.* **1997**, *144*, 1188–1194.
(2) Padhi, A.; Nanjundaswamy, K.; Okada, S.; Goodenough, J. B. *J. Electrochem. Soc.* **1997**, *144*, 1609–1613.
(3) Sun, C. W.; Rajasekhara, S.; Goodenough, J. B.; Zhou, F. *J. Am. Chem. Soc.* **2011**, *133*, 2132–2135.
(4) Aricò, A. S.; Bruce, P.; Scrosati, B.; Tarascon, J. M.; Schalkwijik, W. V. *Nat. Mater.* **2005**, *4*, 366–377.
(5) Tarascon, J. M.; Armand, M. *Nature* **2001**, *414*, 359–496.
(6) Armand, M.; Tarascon, J. M. *Nature* **2008**, *451*, 652–657.
(7) Gibot, P.; Casas-Cabanas, M.; Laffont, L.; Levasseur, S.; Carlach, P.; Hamelet, S.; Tarascon, J. M.; Masquelier, C. *Nat. Mater.* **2008**, *7*, 741–747.
(8) Morgan, D.; Ceder, G.; Saidi, M. Y.; Barker, J.; Swoyer, J.; Huang, H.; Adamson, G. *Chem. Mater.* **2002**, *14*, 4684–4693.
(9) Yin, S. C.; Grondey, H.; Strobel, P.; Anne, M.; Nazar, L. F. *J. Am. Chem. Soc.* **2003**, *125*, 10402–10411.
(10) Kuang, Q.; Zhao, Y. M.; An, X. N.; Liu, J. M.; Dong, Y. Z.; Chen, L. *Electrochim. Acta* **2010**, *55*, 1575–1581.
(11) Dai, C. S.; Chen, Z. Y.; Jin, H. Z.; Hu, X. G. *J. Power Sources* **2010**, *195*, 5775–5779.
(12) Huang, J. S.; Yang, L.; Liu, K. Y.; Tang, Y. F. *J. Power Sources* **2010**, *195*, 5013–5018.
(13) Deng, C.; Zhang, S.; Yang, S. Y.; Gao, Y.; Wu, B.; Ma, L.; Fu, B. L.; Wu, Q.; Liu, F. L. *J. Phys. Chem. C* **2011**, *115*, 15048–15056.
(14) Mateyshina, Yu.G.; Uvarov, N. F. *J. Power Sources* **2011**, *196*, 1494–1497.
(15) Ren, M. M.; Zhou, Z.; Li, Y. Z.; Gao, X. P.; Yan, J. *J. Power Sources* **2006**, *162*, 1357–1362.
(16) Barker, J.; Gover, R. K. B.; Burns, P.; Bryan, A. *J. Electrochem. Soc.* **2007**, *154*, A307–A313.
(17) Ai, D.; Liu, K.; Lu, Z.; Zou, M.; Zeng, D.; Ma, J. *Electrochim. Acta* **2011**, *56*, 2823–2827.
(18) Chen, Y. H.; Zhao, Y. M.; An, X. N.; Liu, J. M.; Dong, Y. Z.; Chen, L. *Electrochim. Acta* **2009**, *54*, 5844–5850.
(19) Liu, S. Q.; Li, S. C.; Huang, K. L.; Chen, Z. H. *Acta Phys. Chim. Sin.* **2007**, *23*, 537–542.
(20) Sato, M.; Ohkawa, H.; Yoshida, K.; Saito, M.; Uematsu, K.; Toda, K. *Solid State Ionics* **2000**, *135*, 137–142.
(21) Xia, Y.; Zhang, W.; Huang, H.; Gan, Y.; Li, C.; Tao, X. *Mater. Sci. Eng., B* **2011**, *176*, 633–639.
(22) Zhang, L. L.; Zhang, X.; Sun, Y. M.; Luo, W.; Hu, X. L.; Wu, X. J.; Huang, Y. H. *J. Electrochem. Soc.* **2011**, *158*, A924–A929.
(23) Huang, H.; Yin, S.; Kerr, T.; Taylor, N.; Nazar, L. F. *Adv. Mater.* **2002**, *14*, 1525–1528.
(24) Bykov, A. B.; Chirkin, A. P.; Demyanets, L. N.; Doronin, S. N.; Genkina, E. A.; Ivanov-Shits, A. K.; Kondratyuk, I. P.; Maksimov, B. A.; Mel'nikov, O. K.; Muradyan, L. N.; Simonov, V. I.; Timofeeva, V. A. *Solid State Ionics* **1990**, *38*, 31–52.
(25) Saïdi, M. Y.; Huang, H.; Swoyer, J. L.; Adamson, G. *J. Power Sources* **2003**, *119−121*, 266–272.
(26) Saïdi, M. Y.; Baker, J.; Huang, H.; Swoyer, J. L.; Adamson, G. *Electrochem. Solid-State Lett.* **2002**, *5*, A149–A151.
(27) Pan, A. Q.; Liu, J.; Zhang, J. G.; Xu, W.; Cao, G. Z.; Nie, Z. M.; Arey, B. W.; Liang, S. Q. *Electrochem. Commun.* **2010**, *12*, 1674–1677.
(28) Shannon, R. D.; Prewitt, C. T. *Acta Crystallogr., Sect. B* **1969**, *25*, 925–946.
(29) Smith, A. J.; Burns, J. C.; Trussler, S.; Dahn, J. R. *J. Electrochem. Soc.* **2010**, *157*, A196–A202.
(30) Xu, K. *Chem. Rev.* **2004**, *104*, 4303–4417.
(31) Ren, M. M.; Zhou, Z.; Gao, X. P. *J. Appl. Electrochem.* **2010**, *40*, 209–213.
(32) Goodenough, J. B.; Kim, Y. *Chem. Mater.* **2010**, *22*, 587–603.
(33) Aurbach, D. *J. Power Sources* **2000**, *89*, 206–218.
(34) Edström, K.; Gustafsson, T.; Thomas, J. O. *Electrochim. Acta* **2004**, *50*, 397–403.